Simulation of a QMS Including the Effects of Pressure in the Electron-Impact Ion Source

Jeyan Sreekumar, Thomas J. Hogan, *Member, IEEE*, and Stephen Taylor

***Abstract*—This paper is concerned with the computer modeling of a quadrupole mass spectrometer (QMS) to include the effect of pressure in the ion source. The paper simulates the spectra over the pressure range from 10^{-6} to 10^{-4} mbar. An important contribution is the development of a novel procedure to include pressure dependence of the ion source to allow better prediction of instrument performance. Electron-impact total ionization cross sections in the ionic current expression are calculated using the binary-encounter-Bethe theory for argon gas. The predicted results show good agreement with the experimental results obtained from a commercial QMS used for residual gas analysis.**

***Index Terms*—Binary-encounter-Bethe (BEB), electron-impact ion source, gas measurement, ionic current, partial pressure, quadrupole mass spectrometer (QMS), quadrupole mass spectrometry, residual gas analyzer.**

I. Introduction

ALTHOUGH mass spectroscopic techniques have been used to study free ions formed in electric discharges and flames, and even ions existing in the upper atmosphere, a more common use of these techniques is to determine the partial pressure of neutral molecules in a residual gas mixture. These neutral molecules are formed into gaseous ions in an ion source. In the process, some form of energy is transferred to the analyte molecules to effect ionization. Ionic current generated in an ion source is pressure dependent and also depends on the ionization cross section of the atoms/molecules.

In the electron ionization (EI) technique, the molecular ions of the analyte are converted into a variety of lower mass fragment ions. The resulting fragmentation pattern, together with residual molecular ions, results in a mass spectrum that can be used as a "fingerprint" to characterize the analyte. This way, the application of mass spectrometers became widespread for residual gas analysis (RGA) in the study of kinetic reactions, biological analysis, biochemistry, explosives, and in the oil and gas industry [1], [2]. Mass spectrometry (MS) has also the potential to provide accurate mass measurements for low molecular weight compounds (gases) to large macromolecules. Increased applications have led to further demand in instrument design and performance.

Manuscript received January 3, 2012; revised March 23, 2012; accepted March 26, 2012. Date of publication July 24, 2012; date of current version October 10, 2012. The Associate Editor coordinating the review process for this paper was Dr. George Xiao.

The authors are with the Department of Electrical Engineering and Electronics, University of Liverpool, Liverpool L69 3GJ, U.K. (e-mail: jeyan@liverpool.ac.uk; t.j.hogan@liverpool.ac.uk; s.taylor@liverpool.ac.uk).

Color versions of one or more of the figures in this paper are available online at http://ieeexplore.ieee.org.

Digital Object Identifier 10.1109/TIM.2012.2202166

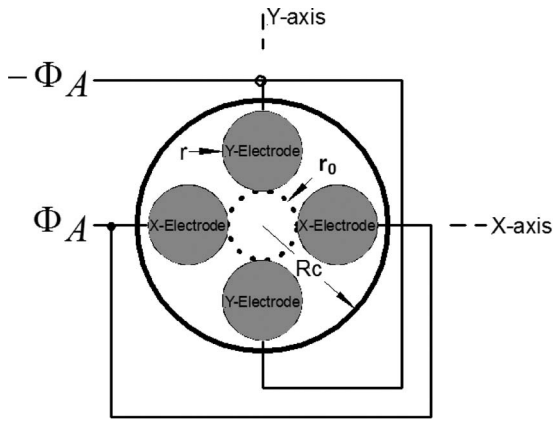

Fig. 1. Cross section of a typical *QMF* using circular electrodes of radius r, central field radius r_0, and enclosure radius R_c, showing the combination of dc (U) and RF (V) drive voltages applied to the x- and y-axis electrodes.

A typical quadrupole mass spectrometer (QMS) consists of a mass analyzer, which has four longitudinal parallel electrodes with an angular spacing of 90°. The ideal electrode form is hyperbolic; however, in practice, circular electrodes are commonly used because of the difficulty in machining electrodes with hyperbolic cross sections [3]. Fig. 1 shows the cross section of a typical quadrupole mass filter (QMF) using circular electrodes. The field in this case closely approximates to the ideal hyperbolic field, provided that the electrode diameter and separation are correctly chosen [4]. However, even a small positioning error or approximation in the shape of electrodes results in nonidealities, which degrade instrument performance [5].

Considerable work has been undertaken to examine QMS performance. In the early studies of Dawson and Whetten [6], [7], numerical computer simulation techniques were employed to integrate the Mathieu equation. A detailed study by Richards *et al.* [8] employed matrix methods to calculate the state transition matrix from the initial conditions of the ion to obtain the position and velocity of an ion at a point of the RF phase. The calculation of ion trajectories by phase-space dynamics using the matrix method to evaluate ion entrance conditions has been discussed by Baril *et al.* [9]. All these works were based on ion trajectory analysis in the 2-D quadrupole field in the plane perpendicular to the four electrodes. Many numerical simulation techniques have been performed to study the theoretical performance characteristics of the QMS. Later research work has continued detailed investigation of mass spectra using computer simulation techniques for both hyperbolic and circular electrodes [10], [11]. The field generated from the circular

electrodes approximately represents the quadrupole field plus the sum of a number of higher order fields, which is termed the multipole field [12]. The relative magnitude of the individual components of the multipole field can be controlled by the ratio of the electrode radius r to the inscribed radius r_0. Subsequent work was carried out to achieve the best performance QMS by altering the ratio r/r_0. Computer simulation has shown that, when operating in Zone 1 of the Mathieu stability diagram, circular electrodes with $r/r_0 = 1.148$ suffer from increased peak width, lower transmission, and low mass tailing than hyperbolic electrodes [11]. More recently, numerical computer simulations operated in Zone 1 have shown improved performance of r/r_0 in the range from 1.125 to 1.130 [11], [13], [14]. Analytical techniques have found the same value of 1.128–1.130 for the r/r_0 ratio for operation in Zone 1 [12]. It was later found that this value is almost the same for operation in Zone 3 of the Mathieu stability diagram [15], [16].

A theoretical understanding of RGA operation at higher pressures is becoming important as small footprint instruments are being increasingly used [17], [18]. Small RGA size can allow operation at higher pressures that permits deployment for applications outside of the laboratory in harsh environments [19].

Reported here is a new approach to include pressure dependence in the ion source to allow better prediction of QMS instrument performance. The binary-encounter-Bethe (BEB) theory was used to calculate from first principles the total ionization cross-sectional values as a function of electron energy [20]–[22]. The BEB theory allows the ion current in the source to be determined as a function of electron emission current, electron energy, and pressure. This approach was then used to model an EI ion source used in a QMS RGA. A commercial QMS residual gas analyzer, MKS MicroVision Plus, was used for the experiments. The predicted results from the model were compared with the experiment.

II. Theory

A. Ionization By Electron Impact

The attributes of the electron-impact ion source make it the most popular choice for many MS instruments. The characteristics that allow widespread usage are reproducible mass spectra and fragmentation of ions, which can provide the structural information of analyte molecules. In an EI ion source, ionic currents are generated by using the EI process, which enables the conversion of electrically neutral molecules into electrically charged molecules. In EI for QMS instruments, electrons are generated through thermionic emission [23] by an electrically heated coil filament to a temperature at which it emits free electrons. The emitted electrons are accelerated with approximately 70 eV forming an electron beam (e-beam) between the filament and the anode trap. The analyte molecule sample is introduced to the ion source normally in a direction perpendicular to the e-beam. Upon interaction between the analyte sample and the e-beam, the neutral molecules are ionized to become radical positive ions [24]. The generated radical positive ions are directed toward the mass analyzer by a positive potential applied to a repeller electrode. The ionization chamber is maintained at a low pressure in order to minimize ion/neutral molecule collisions. The cleavage reactions during the ionization process give rise to fragment ions.

B. Development of the Theoretical Model

When an energetic e-beam passes through a gas containing atoms of a given cross-sectional area, the ionic current (i^+) thus generated in the EI ion source can be expressed as [25]

$$i^+ = \beta\, n_0\, Q_i\, s_l\, I_e \quad [\mathrm{A}] \tag{1}$$

where I_e is an electron (emission) current (in amperes), s_l is an effective electron path length (in meters), Q_i is an ionization cross section $(10^{-10}$ m), n_0 is the density of molecules in the ionization chamber (in m^{-3}), and β is a nondimensional parameter representing the ion extraction efficiency.

1) Electron (Emission) Current I_e: Electrons can be obtained from a hot metal cathode and directed into a vacuum with a wide range of energy values, and this process is termed thermionic emission. The emission of an electron current from a metal surface depends on the temperature of the metal and the applied field strength [26]–[28].

2) Effective Electron Path Length s_l: The determination of the effective electron path length in the ionization chamber is necessary for the evaluation of the ionic current of a given gas component. If there is no axial magnetic field, then the electron traverses a straight-line path across the ionization chamber and the diameter of the ionization chamber can be taken as the effective electron path length. In the presence of an axial magnetic field, electrons move in a helix and the electron path length depends on the size (radius) of the helix. For a helix of diameter d_a (in millimeters), the corresponding maximum possible electron path length is given by [29]

$$l_{\max} = s_l \left(1 + 1.10 \times \frac{10^{-4} d_a^2 H^2}{E_n}\right) \quad [\mathrm{m}] \tag{2}$$

where E_n is the energy of the electrons (in electronvolts), and H is the magnetic field strength (in teslas).

Magnetic field strength H is given by

$$H = \mu_0\, n\, I \quad [\mathrm{T}] \tag{3}$$

where μ_0 is the permeability of free space $(= 4\pi \times 10^{-7}\ \text{H m}^{-1})$, n is the turn density (in m^{-1}), and I is the current flowing through the filament (in amperes).

3) Ionization Cross Section Q_i: The total ionization cross section in the ionic current expression can be calculated using the BEB theory [30]–[32]. The total ionization cross section can be obtained by integrating the differential cross section over the electron energy. The BEB theory, however, uses the orbital binding energy B, the orbital kinetic energy $U = (p^2/2m)$, and the orbital electron occupation number N for the calculation of total ionization cross section for each orbital in the target atom or molecule. The BEB cross section is a function of the kinetic energy of the incident electrons; T can be calculated as

a sum of all the molecular orbitals, as given in the following equations:

$$\sigma_{\mathrm{BEB}} = \frac{4\pi a_0^2 N \left(\frac{B}{R}\right)^2}{t+u+1} \times \left[\frac{\ln t}{2}\left(1-\frac{1}{t^2}\right)+1-\frac{1}{t}-\frac{l_n t}{1+t}\right] \ [10^{-10}\mathrm{m}]$$
$$t = T/B; \quad u = U/B \tag{4}$$

where B is the binding energy (in electronvolts), U is the orbital kinetic energy (in electronvolts), N is the electron occupation number, Q is the dipole constant, a_0 is the Bohr radius ($= 5.29 \times 10^{-11}$ m), and R is the Rydberg energy ($= 13.6$ eV). B, U, N, and Q are the four orbital constants for each orbital.

4) Density of Molecules n_0: In the ionic current equation, the density of molecules in the ionization chamber can be calculated by using the ideal gas law

$$P = n_0 KT \tag{5}$$

where P is the absolute pressure, n_0 is the density of molecules, K is Boltzmann's constant ($= 1.381 \times 10^{-23}$ J K^{-1}), and T is the absolute temperature (in kelvin).

5) Ion Extraction Efficiency β: The ion extraction efficiency β in the ionic current equation can vary from 0.02% to 0.1% for a high-sensitivity source. β depends on a number of factors such as energy homogeneity, beam width, and the mass of the ion [25].

III. Method

The simulation software suite used has been developed in the .Net environment using visual C++ to study the performance of QMS for both hyperbolic and circular electrode QMFs. The computer code QMS2 consists of two programs viz., QMS2-Hyperbolic/QMS2-Field and QMS2-Ion.

The QMS2 model consists of a graphical user interface (GUI) with an ion trajectory computing engine to calculate individual ion trajectories. The solution method for the Mathieu equation [3] in the x- and y-coordinates is carried out by means of numerical integration using a fourth-order Runge–Kutta algorithm. The ion entry conditions into the QMF are also taken into account. The QMS2-Ion program generates a large number of individual ion start conditions and stores them in a binary file, which is read by the QMS2-Hyperbolic/QMS2-Field program. Each ion that enters will have the value of ion initial positions in both the x- and y-axes at the entry to the QMF, ion initial phase with respect to the RF drive, and ion initial velocity along the x-, y-, and z-axes. While executing the program, a file is also generated that has the information of ion energy, ion source radius, ion energy spread, ion beam spread, and filename prefix saved as a text file. A data file with the information of ion energy, ion source radius, ion energy spread, and ion beam spread is also generated in text format, and associated files are generated and stored in a subfolder, i.e., Ion-Files, for the use of the ion source program. The various files generated are also stored in subfolder Ion-Files. Finally, MATLAB is used to postprocess the data and for the generation of the graphical results.

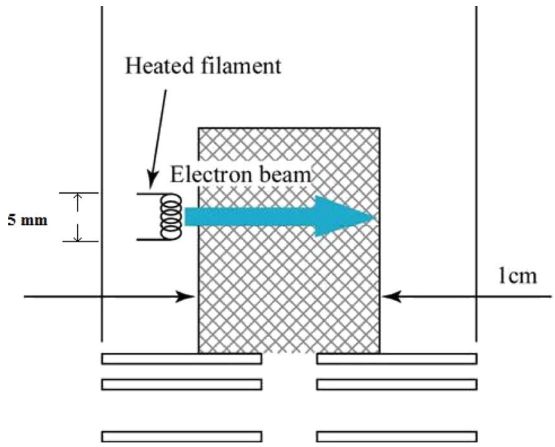

Fig. 2. Typical *EI* ion source of *MKS* MicroVision Plus *RGA* analyzer.

IV. Results and Discussion

A. Experimental Results

Reported here is the experimental analysis of argon gas using a commercial QMS residual gas analyzer, MKS MicroVision Plus.

Fig. 2 shows a schematic of the EI ion source QMS instrument for the MKS analyzer, which is a typical RGA. The e-beam emitted from the heated filament is directed into the mesh ionization cage where it is allowed to interact with the argon gas. Upon interaction between the argon neutral atoms and the e-beam, the neutral argon atoms are ionized to radical positive ions, as described earlier. This instrument is a single-filter analyzer with circular electrodes of 100-mm long, diameter of 6.35 mm, and r_0 of 2.76 mm. It is excited with an RF frequency of 1.8432 MHz, and the exit hole diameter on the EI ion source is 1.1 mm. During the experiment, argon gas was introduced into the vacuum chamber, which is at a base pressure of 7.9×10^{-6} mbar. The electron emission current in the ion source was varied in the range from 0.35 to 1 mA, and the electron energy was set to 70 eV. A fully automated high-stability RF and data acquisition electronic drive unit driven by a PC was used. The drive unit supports fast wide dynamic range of scanning the mass filter electrode voltages and displays the mass spectrum on the PC screen.

Fig. 3 shows a range of experimental mass peaks of argon gas of mass 40 for an emission current of 0.35 mA, electron energy of 70 eV, and ion energy of 8.8 eV showing the variation in peak height with the applied pressure ranges between 2.6×10^{-4} and 1.3×10^{-5} mbar in the vacuum chamber. As expected, the peak height in the mass spectrum increases with the partial pressure of ions in a linear manner.

Fig. 4 shows the total pressure versus the experimental total ionic current for $^{40}Ar^{+}$ with the total pressure in the range from 2.6×10^{-4} to 1.3×10^{-5} mbar for different emission currents of 0.35, 0.45, 0.8, and 1.0 mA. As shown in Fig. 4, the trend lines were constructed to show that the height of experimental mass peaks has linear dependence on the pressure. The linear fit shows good correlation with the experimental total ionic current for different emission currents. The results show that increasing the total pressure in the chamber results

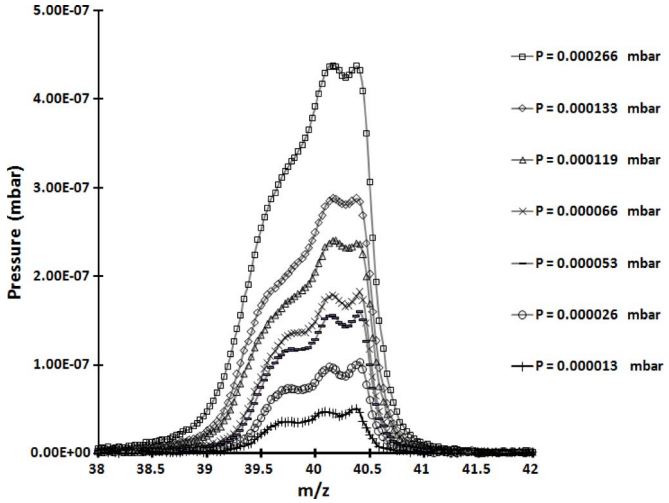

Fig. 3. Experimental mass spectrum of $^{40}Ar^{+}$.

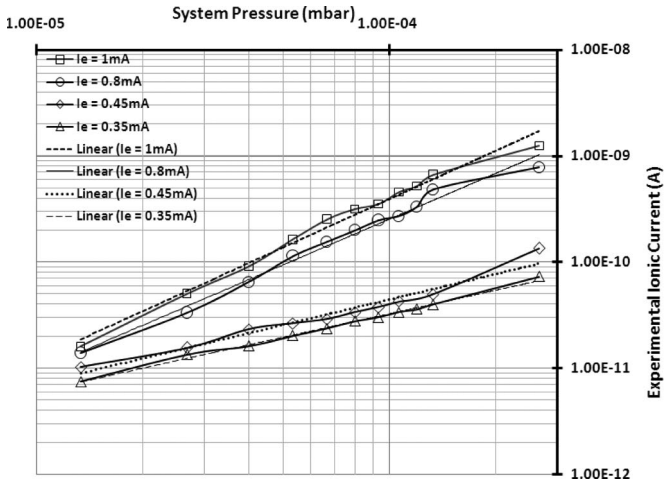

Fig. 4. Experimental argon ionic current with increasing pressure for different electron emission currents I_e.

in an increasing ionic current. The sample pressure correlates directly with the resulting ionic current. Increase in the electron emission current at high pressure results in an increase in the ionization of the neutral species to radical positive ions. As expected, the results show that increasing the emission current produces a higher ionic current. The system displays the mass spectrum on the PC by the displayed pressure (in millibars) on the ordinate. The ionic current generated by the EI ion source in the MKSRGA analyzer was calculated by multiplying the sensitivity of the system (from the instrument provider), which is 1.5×10^{-4} A/mbar $(= 2 \times 10^{-7}$ A/mtorr) by the displayed pressure (in millibars) on the ordinate for the corresponding experimental argon peak.

B. Theoretical Predictions

This section gives the theoretical analysis for the case of argon gas using the equation for calculating ionic current [25] as described earlier.

For a filament length of 5 mm, a turn density of 1000 turns/m, and a filament current of 1.6 mA, the magnetic field strength produced by the heated filament is calculated to be 2×10^{-6} T

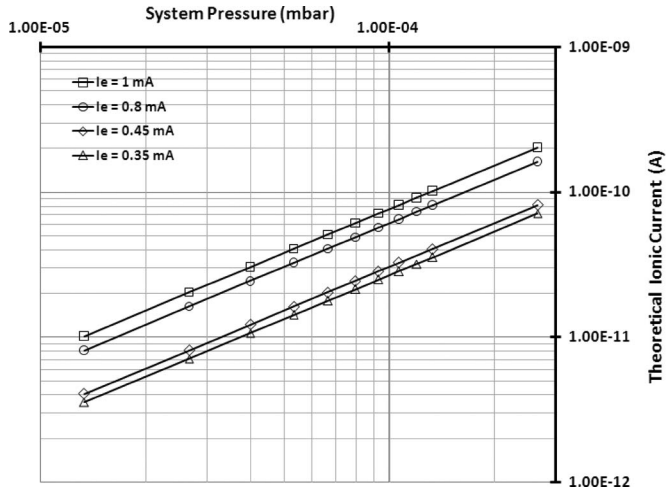

Fig. 5. Predicted argon ionic current with pressure for different values of electron emission current I_e.

using (3). The maximum possible electron length that an electron can achieve due to the application of magnetic field strength [33] is therefore calculated using (2) and found to be 1.54×10^{-10} m, which is a negligible increase in path length compared to the collision chamber length $(1 \times 10^{-2}$ m). Because the magnetic field effect is neglected, the effective electron path length was taken as the length of the collision chamber [28].

Fig. 5 shows the theoretical total ionic current for $^{40}Ar^{+}$ as a function of the total pressure in the range from 2.6×10^{-4} to 1.3×10^{-5} mbar for different emission currents of 0.35, 0.45, 0.80, and 1.00 mA. The total ionic current was calculated by solving the ionic current expression, and the value of the differential ionization of a gas component was taken from the values generated using the BEB theory for different electron energy values. In the calculation of ionic current of argon gas, the differential ionization of a gas component value was taken from published values [34]. From the graph, it is clear that the model predicts that the ion current generated correlates directly with the sample pressure, as found in Fig. 4.

Fig. 6 shows the comparison of the calculated and experimental total ionic currents for argon gas (m/z 40) with the total pressure in the range from 2.6×10^{-4} to 1.3×10^{-5} mbar for emission currents of 0.35 and 0.45 mA. The ionic current was calculated neglecting the axial magnetic field experienced by the heated coil as previously discussed. In Fig. 6(a), the theoretical results show good close agreement with the measured experimental values. In Fig. 6(b) (higher emission current), the trend of the curves is very similar but the values of the experimental ionic current are in error by 1×10^{-11} A. The difference between the experiment and the theory may be related to measurement noise. We consider the agreement reasonable.

C. GUI of Pressure-Dependence QMS2-EI Ion Source Model

Using the above approach, an EI ion source model has been developed, which allows simulated mass spectra to be determined. Input parameters include electron emission current, electron energy, and pressure.

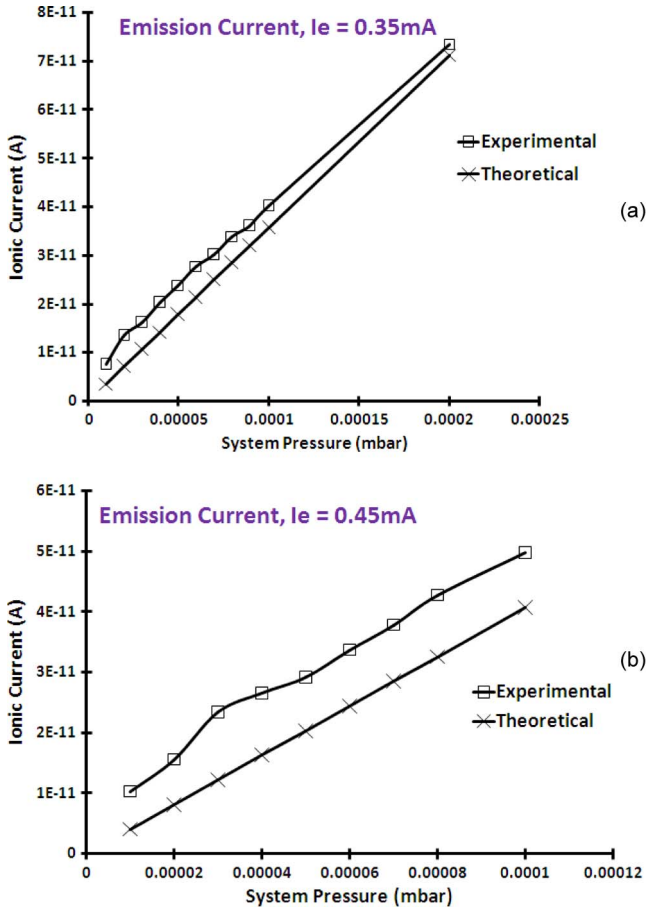

Fig. 6. Comparison of calculated and experimental total ionic currents for $^{40}Ar^{+}$ as a function of system pressure for emission currents (a) $I_e = 0.35$ mA and (b) $I_e = 0.45$ mA.

The model has been developed in the Visual C++ environment to allow better prediction of instrument performance. Previous versions of the QMS2-Ion source model do not support the calculation of ionic current, which has pressure dependence. The new model calculates the ionic current of the given gas component and takes the value of the ionization cross section of a gas component from the values generated using the BEB theory for different electron energy values.

Fig. 7 shows simulated mass peaks of argon gas of (m/z 40) calculated using the QMS2-Hyperbolic and QMS2-EI ion source pressure-dependence programs operated in stability Zone 1 ($a = 0.237$ and $q = 0.706$). The computer simulation test conditions are given in Table I. The figure shows an increase in the peak height and, consequently, an increase in the peak width as the total pressure is maintained between the pressure range 2.6×10^{-4} to 1.3×10^{-5} mbar.

Fig. 8 shows the comparison of the simulated and experimental mass peaks for $^{40}Ar^{+}$. The generated ionic current is input into the QMF simulator and the mass spectral peak (partial pressure) for a particular gas determined and compared with the experiment. The experimental mass peak for $^{40}Ar^{+}$ ions obtained from a commercial QMS residual gas analyzer (MKS MicroVision Plus RGA) operated for an electron current of 0.35 mA with a pressure is 6.6×10^{-5} mbar. The ion energy was set to 8.8 eV. The simulated mass peak for $^{40}Ar^{+}$ ions is generated using the QMS2-Hyperbolic and QMS2-EI ion source pressure-dependence programs. The input parameters for the ion source and the QMF are the same as those in the experiment as described above. The simulated mass peaks of $^{40}Ar^{+}$ show reasonable agreement with the experimental mass peaks.

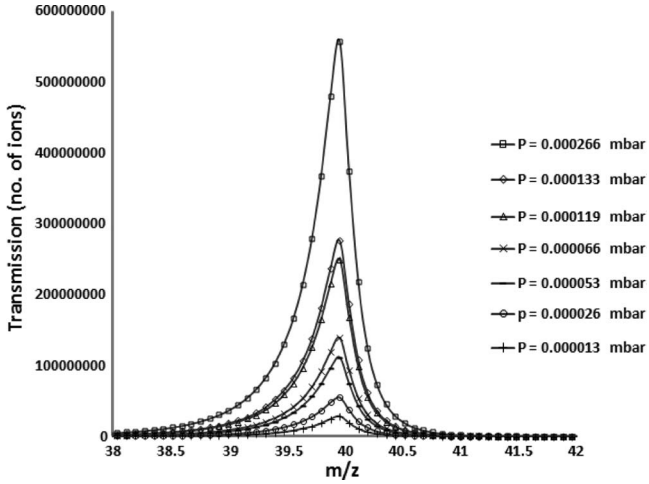

Fig. 7. Simulated mass spectrum of $^{40}Ar^{+}$.

TABLE I
QMS2 COMPUTER SIMULATION TEST CONDITIONS

QMF PARAMETER	CONDITION
Length	100 mm
r_0	2.76 mm
Frequency	1.8432 MHz
U/V	100
Detector radius	10 mm
Ion Source	
Ion energy	8.8 eV
Ion source radius	0.55 mm
Ion energy spread	0
Ion angular spread	0
Ion species	40 m/z

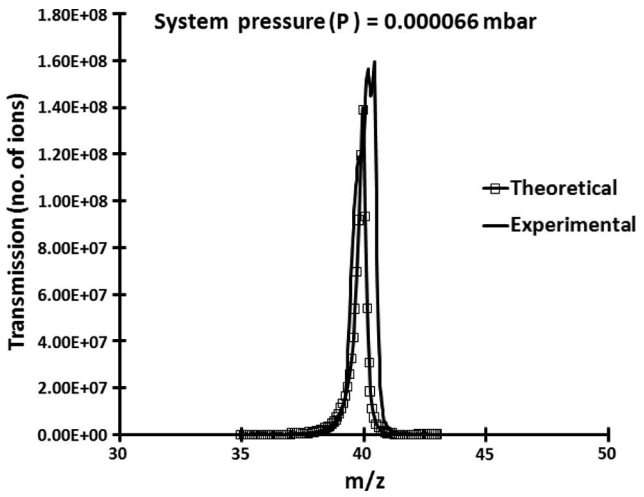

Fig. 8. Comparison of simulated and experimental mass spectra of $^{40}Ar^{+}$.

V. Conclusion

A QMS2-EI ion source pressure-dependence theoretical model has been developed using the visual C++ environment. The model as a function of electron energy calculates the electron-impact total ionization cross sections using the BEB theory. The QMS2-EI ion source pressure-dependence model allows simulated mass spectra to be determined, including the effects of electron emission current, electron energy, and pressure. The calculated theoretical ionic currents are compared with the ionic current of the experimental results obtained from a commercial QMS residual gas analyzer and show reasonable agreement. Successful simulation tests have been also carried for argon gas in the pressure range from 10^{-6} to 10^{-4} mbar for different emission currents 0.35, 0.45, 0.80, and 1 mA. The predicted results of argon match well with the experimental results obtained using a commercial QMS RGA. Future work will focus upon testing the model with different gases and quantifying the performance characteristics experimentally. In particular, the model will be used to investigate different modes of QMS operation, e.g., for "soft ionization" MS applications. In this case, mass spectra are obtained at low values of electron energy in the EI source, which can provide a further means of atomic and molecular analysis. The theoretical model provided by this paper offers a method of QMS simulation for such applications.

References

[1] R. K. Waits, "Semiconductor and thin film applications of a quadrupole mass spectrometer," *J. Vac. Sci. Technol. A, Vac. Surf. Films*, vol. 17, no. 4, pp. 1469–1478, Jul. 1999.

[2] J. H. Batey, "Quadrupole gas analyzers," *Vacuum*, vol. 37, pp. 659–668, 1987.

[3] P. H. Dawson, "Principles of operation," in *Quadrupole Mass Spectrometry and its Applications*. Amsterdam, The Netherlands: Elsevier, 1976, pp. 9–64.

[4] T. J. Hogan and S. Taylor, "Performance simulation of a quadrupole mass filter operating in the first and third stability zones," *IEEE Trans. Instrum. Meas.*, vol. 57, no. 3, pp. 498–508, Mar. 2008.

[5] N. R. Whetten and P. H. Dawson, "Some causes of poor peak shapes in quadrupole field mass analyzers," *J. Vac. Sci. Technol.*, vol. 6, no. 1, pp. 100–103, Jan. 1969.

[6] P. H. Dawson and N. R. Whetten, "Non-linear resonances in quadrupole mass spectrometers due to imperfect fields I. the quadrupole ion trap," *Int. J. Mass Spectrom. Ion Phys.*, vol. 2, no. 1, pp. 45–59, Jan. 1969.

[7] P. H. Dawson and N. R. Whetten, "Non-linear resonances in quadrupole mass spectrometers due to imperfect fields, II. The quadrupole mass filter and the monopole mass spectrometer," *Int. J. Mass Spectrom. Ion Phys.*, vol. 3, no. 1/2, p. 1-12, Sep. 1969.

[8] J. A. Richards, R. M. Huey, and J. Hiller, "A new operating mode for the quadrupole mass filter," *Int. J. Mass Spectrom. Ion Phys.*, vol. 12, no. 4, pp. 317–339, Nov. 1973.

[9] M. Baril, R. Le, and P. Marchand, "An improved and accurate method for the calculation of trajectories in quadrupole mass filters and ion traps using phase space dynamics," *Int. J. Mass Spectrom. Ion Process.*, vol. 98, no. 1, pp. 87–97, Jun. 1990.

[10] J. Gibson, S. Taylor, and J. H. Leck, "Detailed simulation of mass spectra for quadrupole mass spectrometer systems," *J. Vac. Sci. Technol. A, Vac. Surf. Films*, vol. 18, no. 1, pp. 237–243, Jan./Feb. 2000.

[11] J. R. Gibson and S. Taylor, "Prediction of quadrupole mass filter performance for hyperbolic and circular cross section electrodes," *Rapid Commun. Mass Spectrom.*, vol. 14, no. 18, pp. 1669–1673, Jul. 2000.

[12] D. J. Douglas and N. V. Konenkov, "Influence of the 6th and 10th spatial harmonics on the peak shape of a quadrupole mass filter with round rods," *Rapid Commun. Mass Spectrom.*, vol. 16, no. 2, pp. 1425–1431, May 2002.

[13] J. R. Gibson and S. Taylor, "Numerical investigation of the effect of electrode size on the behaviour of quadrupole mass filters," *Rapid Commun. Mass Spectrom.*, vol. 15, no. 20, pp. 1960–1964, Oct. 2001.

[14] D. R. Denison, "Operating parameters of a quadrupole in a grounded cylindrical housing," *J. Vac. Sci. Technol.*, vol. 8, no. 1, pp. 266–269, Jan. 1971.

[15] T. J. Hogan and S. Taylor, "Effects of mechanical tolerances on qmf performance for operation in the third stability zone," *IEEE Trans. Instrum. Meas.*, vol. 59, no. 7, pp. 1933–1940, Jul. 2010.

[16] J. Sreekumar, T. J. Hogan, S. Taylor, P. Turner, and C. Knott, "A quadrupole mass spectrometer for resolution of low mass isotopes," *J. Amer. Soc. Mass Spectrom.*, vol. 21, no. 8, pp. 1364–1370, Aug. 2010.

[17] R. J. Ferran and S. Boumsellek, "High-pressure effects in miniature arrays of quadrupole analyzers for residual gas analysis from 1E-9 to 1E-2 torr," *J. Vac. Sci. Technol. A, Vac. Surf. Films*, vol. 14, no. 3, pp. 1258–1265, May 1996.

[18] L. F. Velasquez-García, B. Gassend, and A. I. Akinwande, "CNT-based MEMS ionizers for portable mass spectrometry applications," *J. Microelectromech. Syst.*, vol. 19, no. 3, pp. 484–493, 2010.

[19] B. Brkic, N. France, and S. Taylor, "Oil-in-water monitoring using membrane inlet mass spectrometry," *Anal. Chem.*, vol. 83, no. 16, pp. 6230–6236, Aug. 2011.

[20] K. K. Irikura, Y.-K. Kim, and M. A. Ali, "Electron-impact total ionization cross sections of hydrocarbon ions," *J. Res. Nat. Inst. Stand. Technol.*, vol. 107, no. 1, pp. 63–67, Jan./Feb. 2002.

[21] G. E. Scott and K. K. Irikura, "Performance of binary-encounter-Bethe (BEB) theory for electron-impact ionization cross sections of molecules containing heavy elements ($Z > 10$)," *Surf. Interf. Anal.*, vol. 37, no. 11, pp. 973–977, Nov. 2005.

[22] Y.-K. Kim, W. Hwang, N. M. Weinberger, M. A. Ali, and M. E. Rudd, "Electron-impact ionization cross sections of atmospheric molecules," *J. Chem. Phys.*, vol. 106, no. 3, pp. 1026–1033, Jan. 1997.

[23] O. W. Richardson, *Thermionic Emission from Hot Bodies*. Seaside, OR: Watchmaker Publ., 2003, pp. 1–196.

[24] F. B. Dunning, "Study of low-energy electron-molecule interactions using Rydberg atoms," *J. Phys. Chem.*, vol. 91, no. 9, pp. 2244–2249, Apr. 1987.

[25] C. A. McDowell, *Mass Spectrometry*. Huntington, NY: Krieger, 1979, pp. 76–77.

[26] V. Nemchinsky, "Simple algorithm to calculate t–f electron emission current density," *IEEE Trans. Dielect. Elect. Insul.*, vol. 11, no. 4, pp. 551–553, Aug. 2004.

[27] E. Guth and C. J. Mullin, "Electron emission of metals in electric fields, iii the transition from thermionic to cold emission," *Phys. Rev. A*, vol. 61, no. 5/6, pp. 339–348, Mar. 1942.

[28] W. W. Dolan and W. P. Dyke, "Temperature-and-field emission of electrons from metals," *Phys. Rev. A*, vol. 95, no. 2, pp. 327–332, Jul. 1954.

[29] H. S. W. Massey and E. H. S. Burhop, *Electronic and Ionic Impact Phenomena*. London, U.K.: Oxford Univ. Press, 1969, pp. 1–26.

[30] Y.-K. Kim and M. E. Rudd, "Binary-encounter-dipole model for electron-impact ionization," *Phys. Rev. A*, vol. 50, no. 5, pp. 3954–3967, Nov. 1994.

[31] Y.-K. Kim, J. P. Santos, and F. Parente, "Extension of the binary-encounter-dipole model to relativistic incident electrons," *Phys. Rev. A*, vol. 62, no. 5, pp. 710–052, Oct. 2000.

[32] M. A. Ali and Y.-K. Kim, "Total ionization cross sections of Cl and Cl2 by electron impact," *Surf. Interf. Anal.*, vol. 37, no. 11, pp. 969–972, Nov. 2005.

[33] R. K. Asundi, "Electron path length in collision experiments," *Proc. Phys. Soc.*, vol. 82, no. 3, pp. 372–374, Sep. 1963.

[34] M. A. Ali and P. M. Stone, "Electron impact ionization of metastable rare gases: He, Ne and Ar," *Int. J. Mass Spectrom.*, vol. 271, no. 1–3, pp. 51–57, Apr. 2008.

Jeyan Sreekumar received the B.Eng. degree from Anna University, Chennai, India, in 2006 and the M.Sc. and Ph.D. degrees from the University of Liverpool, Liverpool, U.K., in 2007 and 2011, respectively.

He is currently a Knowledge Transfer Partnerships Research Associate with the Department of Electrical Engineering and Electronics, University of Liverpool and Advanced Sensors Ltd., Northern Ireland. His professional interests include mass spectrometry with a specific interest in its application to oil-in-water analysis. Research interests include numerical modeling of the QMS, particularly that of the ionization process.

Dr. Sreekumar is a member of The Institute of Engineering and Technology (MIET), a Graduate Member of the Energy Institute (GradEI), and also a member of the British Mass Spectrometry Society and The Chromatographic Society.

Thomas J. Hogan (M'09) obtained the academic qualifications for Chartered Engineer (electrical and electronic) in 1971 and received the M.Sc. degree in microelectronics from the University of Bolton, Bolton, U.K. and the University of Northumbria, Newcastle, U.K., in 2004. He is currently an External Student with the Department of Electrical Engineering and Electronics, University of Liverpool, Liverpool, U.K.

He is also an Independent Consultant Engineer in Cambridge, U.K. and has acted for a number blue chip companies on the design of bespoke electronic and software systems, including computer graphics, satellite imaging, scientific instrumentation, and laser systems. His professional interests include instrumentation, automotive, and embedded control. Research interests include numerical simulation, instrumentation, and distributed microprocessor systems.

Mr. Hogan is also a Chartered Engineer (CEng), European Engineer (EUR ING), and a member of The Institute of Engineering and Technology (MIET).

Stephen Taylor received the B.Sc. degree from Imperial College London, London, U.K., in 1978 and the M.Eng. and Ph.D. degrees from the University of Liverpool, Liverpool, U.K., in 1983 and 1988, respectively.

He is currently a Professor of physical electronics and the Head of the Mass Spectrometry Group in the Department of Electrical Engineering and Electronics, University of Liverpool. Teaching duties include courses in electromagnetics and MEMS Design. He is the author or coauthor of more than 220 articles, patents, or publications in the open scientific literature. In 1995, he invented and codeveloped the (then) world's smallest mass spectrometer and the first to be microengineered in silicon.

Dr. Taylor is a member of the Organizing Committee for the RGA Users Group and a member of the Program Committee for the Harsh Environment Mass Spectrometry Conference. He is a Guest Editor of the Journal of American Society for Mass Spectrometry. He has acted as Consultant to several U.K. companies and is a Director of a university start-up company. He is a Chartered Engineer (CEng), a Fellow of The Institute of Engineering and Technology (FIET), and a Fellow of the Electrical Research Association (FERA).